Efficient Quercetin Sensor Utilizing Chitosan-Modified Carboxylated MWCNTs for Fast and Accurate Analysis

Mengge Duan[a], Yu Sun[a], Shuang Ma[a], Xiao Liu[a], Qingtong Li[a], Chunjing Zhang*[a,b], Qingfang Zhen[c] and Haijun Pang[c]

[a]*College of Pharmaceutical Sciences, Heilongjiang University of Chinese Medicine, Harbin 150040, P. R. China*

[b]*Key Laboratory of Optic-electric Sensing and Analytical Chemistry for Life Science, MOE*

[c]*School of Materials Science and Chemical Engineering, Harbin University of Science and Technology, Harbin 150040, China.*

*To whom correspondence should be addressed.

E-mail: zhangcj922@163.com (C.J. Zhang).

Section 1 Additional Experimental Section

I. Materials

All chemicals are of analytical purity and have not been subjected to a further purification process. Multi-walled carbon nanotubes (MWCNT, >95%), chitosan (CS), 4-vinyl pyridine (4-VP), Quercetin (Qu), sodium sulfate (Na_2SO_4), zinc chloride ($ZnCl_2$), sodium citrate ($C_6H_5Na_3O_7$) were purchased from Aladdin. Rutin (Ru) was obtained from Shanghai Dibo Biotechnology Co., Ltd. Baicalin (Bn), Luteolin (Lu), acetonitrile (CH_3CN), N, N-Dimethylformamide (DMF), ethylene glycol dimethacrylate (EGDMA), 2,2'-azobis (2-methylpropionitrile) (AIBN) were purchased from Rhawn. Glacial acetic acid (GAA), methanol (MeOH), potassium chloride (KCl, 99.5%), magnesium chloride ($MgCl_2$), cobaltous nitrate ($Co(NO_3)_2 \cdot 6H_2O$) were purchased from Tianjin Tianli Chemical Reagent Co., Ltd. Glassy carbon electrode was obtained from Shanghai Yueci Electronic Technology Co., Ltd. Reference electrode (Ag/AgCl (3.0 M KCl)) and counter electrode (platinum wire) were obtained from Shanghai Chenhua Co., Ltd.

II. Instruments

All the electrochemical tests were carried out in a three-electrode testing system (CHI760E electrochemical workstation, Chenhua, Shanghai), where the glassy carbon electrode (3.0 mM in diameter) as a working electrode, a commercial Ag/AgCl (3.0 M KCl) as reference electrode and platinum wire as counter electrode. The FT-IR spectra were obtained with a Bruker Tensor II spectrometer (Bruker, Germany). The surface structures and morphology of the samples were characterized by a field-emission scanning electron microscopy (FE-SEM) (Hitachi, SU8000). X-ray photoelectron spectroscopy (XPS) was obtained with Thermo Scientific K-Alpha XPS spectrometer

III. Atomic Interaction Model Method

All calculations were carried out with the ORCA 6.0.0 software package[1]. The Becke's three-parameter hybrid exchange functionals and the Lee-Yang-Parr correlation functional (B3LYP)[2] was adopted for all calculations in combination with the D3 version of Grimme's dispersion with Becke-Johnson damping (DFT-D3BJ)[3]. For geometry optimization, the def2-SVP basis set[4] and auxiliary def2/J basis[5] were used. The single point energy calculations were performed with def2-TZVP[6] basis set and auxiliary def2/J basis[5]. The Solvation Model Density (SMD) implicit solvation mode[7] was used to account for the solvation effect when performing all the calculations. The diagram of HOMO/LUMO, Electrostatic Potential (ESP)[8] and Reduced density gradient (RDG)[9] was visualized by the Multiwfn and VMD software[10,11].

IV. General Material characterization and electrochemical test methods

The differential pulse voltammetry (DPV), cyclic voltammetry (CV), current-time method (i-t) and electrochemical impedance spectroscopy (EIS) were performed with a CHI-760E electrochemical workstation (Shanghai ChenHua Instruments Co, China). A conventional three-electrode system was employed for the electrochemical detection, which was composed of a modified glass carbon electrode (GCE, 3 mm in diameter) as the working electrode, a platinum wire electrode as the counter electrode, and a saturated calomel electrode as the reference electrode.

Cyclic voltammogram (CV) and differential pulse voltammogram (DPV) measurements were carried out in a three-electrode cell. 10 mL of 0.1 M PBS was added into the electrochemical cell. The CVs were performed in the range of 0–0.8 V. The DPVs were recorded in the range of 0–0.8 V with the parameters of increment potential, 0.004 V; pulse amplitude, 0.05 V; pulse width, 0.05 s; sample width, 0.0167 s; pulse period, 0.2 s; quiet time, 2 s.

V. Detailed calculation process of electroactive surface area for the MIP composite

The electroactive surface area of the MIP composite was assessed by conducting cyclic voltammetry (CV) measurements in a electrolyte of 0.1 M KCl and 5 mM $[Fe(CN)_6]^{3-/4-}$, using varying scan rates ranging from 10 to 100 mV s-1. Based on the linear equation $I_{pa} = 3.643v^{1/2} - 4.609$, $R^2 = 0.996$, the effective surface area of the MIP-CS-CMWCNTs composite is determined using the following equation (Eq S1) [12].

$$I_{pa} = 2.69\times10^5\, n^{3/2}\, A_{eff}\, D_0^{1/2}\, C\, v^{1/2} \qquad \text{(S1)}$$

The term $v^{1/2}$ is the square root of the scan rate, while C indicates the concentration of $[Fe(CN)_6]^{3-/4-}$. Additionally, D_0 stands for the diffusion coefficient, A denotes the electroactive surface area of the electrode, n represents the electron number, and I_{pa} signifies the anodic peak current. Specifically for $[Fe(CN)_6]^{3-/4-}$, the diffusion coefficient D_0 is 7.6×10^{-6} cm^2/s, and the electron number n is 1.

VI. Detailed relationship and calculation process of the anodic (E_{pa}) and cathodic (E_{pc}) peaks and the scan rates for of the MIP composite

The peak potentials of the anodic (E_{pa}) and cathodic (E_{pc}) peaks exhibited a linear plot with the natural logarithm of the scan rates (lnv). The equations obtained from linear regression were as follows: $E_{pa} = 0.029 \ln v + 0.219$, R = 0.999; $E_{pc} = -0.018 \ln v + 0.314$, R = -0.991. The dynamic parameters can be computed utilizing following equation[13], specifically Eq S2 and S3:

$$E_{pa}=E^0 + RT \ln v / (1-\alpha)\, nF \qquad \text{(S2)}$$

$$E_{pc}=E^0 - RT \ln v / \alpha nF \tag{S3}$$

In this context, α represents the charge transfer coefficient, n denotes the number of transferred electrons, v stands for the scan rate, E^0 indicates the formal standard potential, and the remaining parameters are considered in their typical terms. The values of α and n were calculated as 0.62 and 2.30 (≈ 2). Based on the findings from the pH impact section, it can be inferred that the redox reaction of Qu involves the participation of two electrons and two protons. Following the equation: $I_{pa} = n^2F^2vA\Gamma/ 4RT$, where n denotes the quantity of electrons involved in the transfer, F stands for the Faraday constant, v represents the scan rate, A is the electroactive surface area of the electrode, and Γ indicates the surface concentration of the electroactive substance. The calculated average surface coverage of Qu on the modified electrode surface was found to be $\Gamma = 2.88 \times 10^{-9}$ mol cm^{-2}. The outcome indicated that the MIP-CS-CMWCNTs composite enhanced electroactive surface area and promoted the electron transfer.

VII. Information on the types of interferents test

In this experiment, three types of interfering substances were used. Firstly, Rutin (Ru), Baicalin (Ba), and Luteolin (Lu) were chosen as interferents due to their structural similarity to quercetin (Qu) and their common presence as active components in traditional Chinese medicines. Secondly, since quercetin is widely found in fruits, vegetables, tea, and pharmaceuticals, and sodium citrate ($C_6H_5Na_3O_7$) is commonly used as a food additive (e.g., acidity regulator, stabilizer) or as a metabolite in biological samples (such as urine and blood), there is a possibility that they coexist in detection systems; hence, sodium citrate was also selected as an interferent. Lastly, considering that quercetin may be used as a pharmaceutical ingredient in human environments, where various inorganic ions are naturally present, several common inorganic salts—Na_2SO_4, $ZnCl_2$, $MgCl_2$, $Co(NO_3)_2\cdot 6H_2O$, and KCl—were introduced as the third category of interfering substances. The concentration of sodium citrate was 20 times that of the target analyte, the concentration of inorganic ions was 40 times that of the target analyte, and the flavonoid concentration including Ru, Baicalin Ba, and Lu was the same as that of the target analyte.

Section 2 Additional Figures

I. The FT-IR spectra of EGDMA, Qu, 4-vp and MIPs

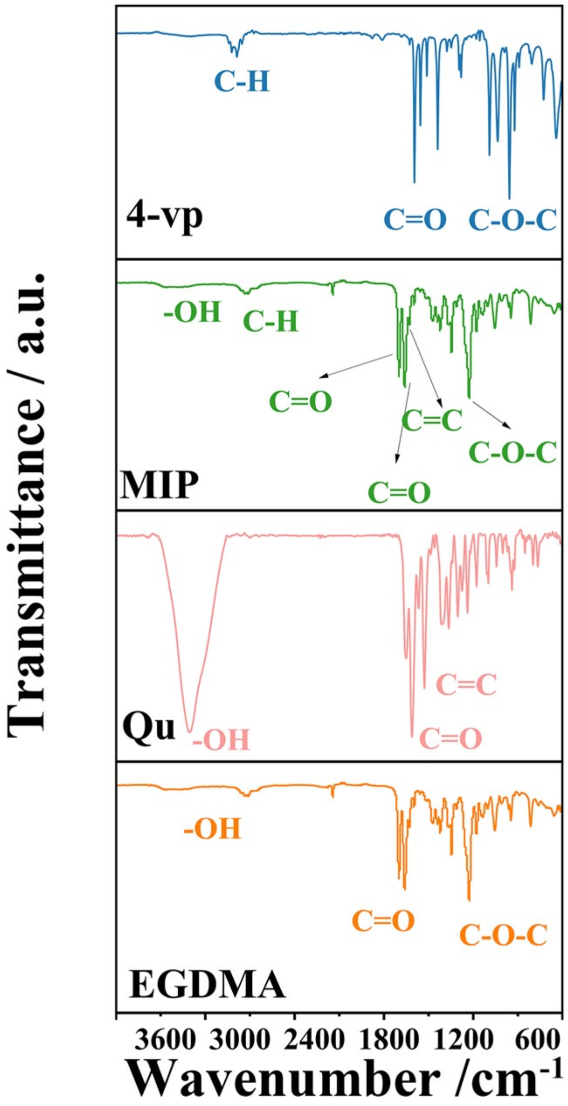

Fig. S1 The FT-IR spectra of EGDMA, Qu, 4-vp and MIPs

II. XPS survey of the CS-CMWCNTs

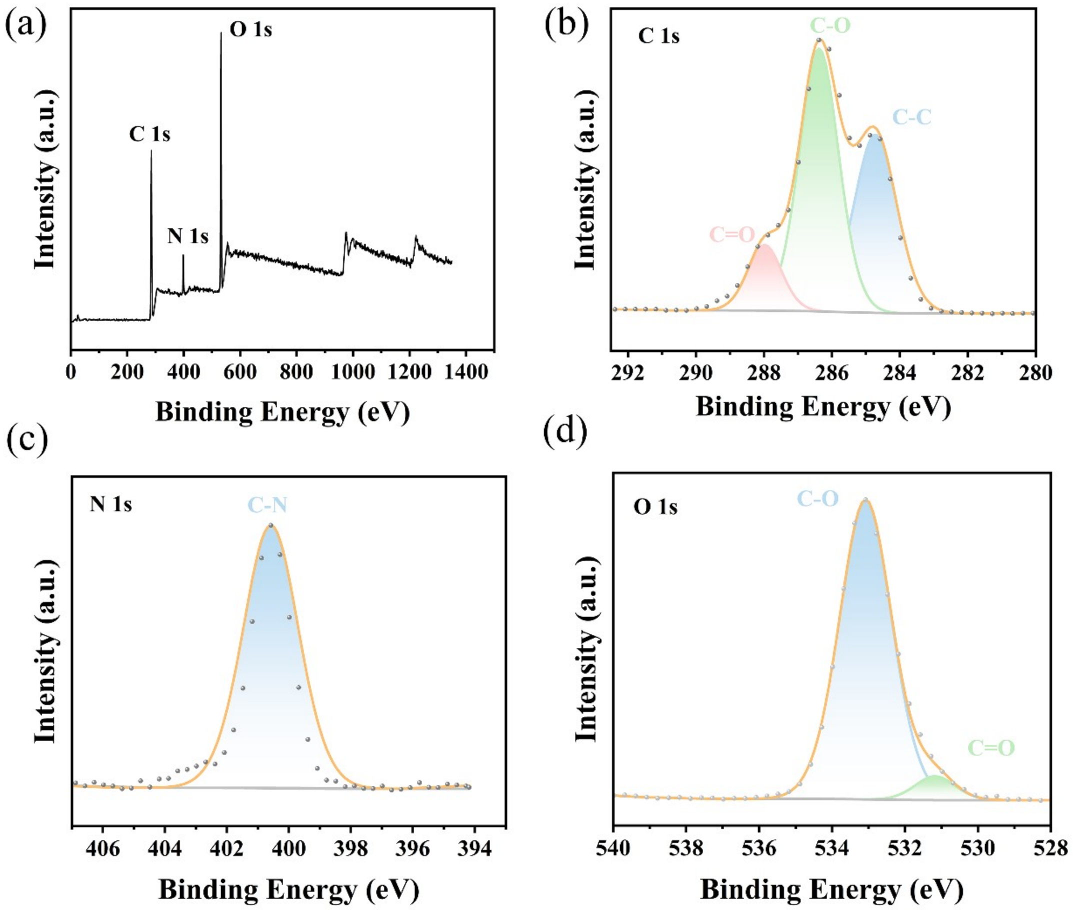

Fig. S2 (a) XPS survey of the CS-CMWCNTs; High-resolution XPS spectra of C 1s (b), N 1s (c), O 1s (d) of CS-CMWCNTs.

III. The long-term stability of the MIP-CS-CMWCNTs/GCE

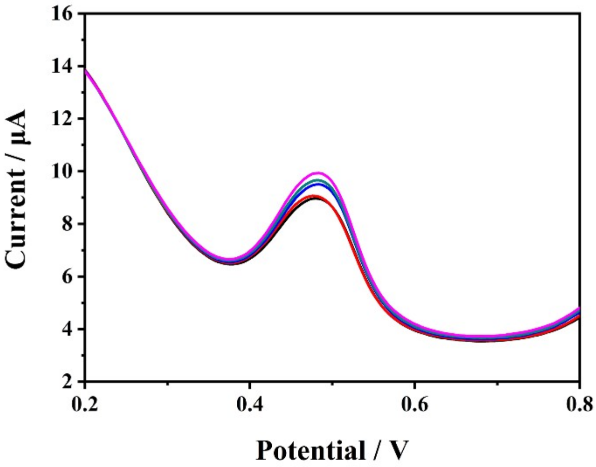

Fig. S3 The long-term stability of the MIP-CS-CMWCNTs/GCE under DPV

Section 3 Additional Tables

Table S1 Effect of the amount of 4-vp on the peak current by one-sample t-test method ($\bar{x} \pm s$, $n=5$, s)

Group	Current (μA)
200	$3.51 \pm 0.15^{**}$
400	$4.37 \pm 0.28^{**}$
600	$1.99 \pm 0.07^{**}$
800	$1.65 \pm 0.12^{**}$
1000	$1.53 \pm 0.14^{**}$

Note: Compared with the 400 group, $^{**}p < 0.01$

Table S2 Effect of elution time on the peak current by one-sample t-test method ($\bar{x} \pm s$, $n=5$, s)

Group	Current (μA)
1	$1.823 \pm 0.55^{**}$
2	$1.86 \pm 0.58^{**}$
3	$2.83 \pm 0.52^{**}$
4	$4.60 \pm 0.30^{**}$
5	$3.22 \pm 0.24^{**}$

Note: Compared with the 4 group, $^{**}p < 0.01$

Section 4 Additional References

References

1. F. Neese, F. Wennmohs, U. Becker, C. Riplinger. The ORCA quantum chemistry program package, *J. Chem. Phys*. 152 (2020) 224108.

2. V. Barone. In: Recent Advances in Density Functional Methods, Part I, edited by D. P.

Chong, World Scientific Publ. Co., Singapore (1996) (cited on pages 19, 277, 278).

3. S. Grimme, S. Ehrlich, L. Goerigk. Effect of the damping function in dispersion corrected density functional theory, *J. Comput. Chem.* 32 (2011) 1456–1465.
4. F. Weigend, R. Ahlrichs. Balanced basis sets of split valence, triple zeta valence and quadruple zeta valence quality for H to Rn: Design and assessment of accuracy, *Phys. Chem. Chem. Phys.* 7 (2005) 3297.
5. F. Weigend. Accurate Coulomb-fitting basis sets for H to Rn, Phys. Chem. Chem. Phys. 8 (2006) 1057.
6. F. Weigend, R. Ahlrichs. Balanced basis sets of split valence, triple zeta valence and quadruple zeta valence quality for H to Rn: Design and assessment of accuracy, *Phys. Chem. Chem. Phys.* 7 (2005) 3297.
7. A. V. Marenich, C. J. Cramer, D. G. Truhlar. Universal solvation model based on solute electron density and on a continuum model of the solvent defined by the bulk dielectric constant and atomic surface tensions, *J. Phys. Chem. B* 113 (2009) 6378.
8. J. S. Murray, P. Politzer. Electrostatic Potentials: Chemical Applications, https://doi.org/10.1002/0470845015.cca014 (2002).
9. T. Lu, Q. Chen. Visualization Analysis of Weak Interactions in Chemical Systems, In: M. Yanez, R. J. Boyd (eds.), Comprehensive Computational Chemistry, vol. 2, *Elsevier, Oxford* (2024) 240–264.
10. T. Lu, F. Chen. Multiwfn: A multifunctional wavefunction analyzer, *J. Comput. Chem.* 33 (2012) 580–592.
11. W. Humphrey, A. Dalke, K. Schulten. VMD – Visual Molecular Dynamics, *J. Mol. Graph.* 14 (1996) 33
12. M.Z.H. Khan, X. Liu, Y. Tang, J. Zhu, W. Hu, X. Liu, A glassy carbon electrode modified with a composite consisting of gold nanoparticle, reduced graphene oxide and poly (L-arginine) for simultaneous voltammetric determination of dopamine, serotonin and L-tryptophan, *Microchim. Acta.* 2018, **185**, 439.
13. E. Laviron, General expression of the linear potential sweep voltammogram in the case of diffusionless electrochemical systems, *J. Electroanal. Chem. Interfacial Electrochem.* 1979, **101**, 19-28.